Theoretical modelling of InP based photo detector for hydrogen fluoride gas detection in short wavelength region

T. K. PARASHAR, R. K. LAL[a,*]
University Polytechnic, Birla Institute of Technology, MESRA, Ranchi, India
[a]Department of Electronics and Communication Engineering, Birla Institute of Technology, MESRA, Ranchi, India

Paper reviews a generic model of InP/InAsSb based photovoltaic gas detector. The model has been applied to characterise a photovoltaic detector for 1.3-1.5μm region. Besides of the characterisation, the effect of trap level and N_t-sigma product on R_0A and detectivity has been investigated detector for HF gas detection. High detectivity and Quantum efficiency obtained on the basis of this model lies in wavelength range 1.25-1.5 μm reveals that this detector is best suited for detection of hydrogen fluoride (HF).

(Received June 24, 2011; accepted July 25, 2011)

Keywords: Gas Detector, HF detector, Zero bias resistance-area products, Detectivity

1. Introduction

A plenty of gases are found in the earth. These gases affect our life in different ways. Some of them (like, Oxygen) are not only blesses life to human being, but also provides the various direct and indirect advantages in industrial and environmental applications. Whereas, on the other hand, breath of some gases (like MIC in Bhopal Gas Tragedy) can even takes the life of several thousand peoples within a small time span. Spreading of such harmful and dangerous toxic gases due to mishandling or any other reason need to be detected, so that quick actions can be taken in time to avoid any serious injury and save human life. Many gas sensors are developed on by various scientists and researchers [1-5] and exist in market but still the investigations for the development of reliable photo detectors tuned to the characteristic wavelength of a toxic gas are going on. Photodetector is a most important part of any gas sensor because overall performance of gas sensor lies on the performance and quality of the photodetector. Computer aided modeling of gas detector is extremely contribute not only to improve the quality of existing photodetector, but also to investigate some novel, high performance gas detectors. In the present paper, we report a model to characterize an InP based photo detector for HF gas detection. However the basic aim of our paper is not only to obtain the characteristic parameter but also to study the effect of material parameter (which could be affected and alter by intentional controlled doping at the time of fabrication such as e_t and N_t-sigma product to tune it for HF gas detection. This band engineering is reported earlier by Prof P. Chakrabarti et al [6]. Our attempt is to utilise such modelling for HF gas detection, whose Characteristic wavelength (1.3 μm) lies in SWIR region. Hydrofluoric acid is extremely corrosive and a contact poison. It should be handled with extreme care, beyond that accorded to other mineral acids, in part because of its low dissociation constant, which allows HF to penetrate tissue more quickly. It is used in certain specific chemical processes, such as wafer cleaning in the microelectronics industry, TFT-LCD manufacturing, and utilization for etching procedures on circuit boards and as a glass thinner. Nevertheless, the noxious characteristics of hydrofluoric acid can cause tremendous problems in the human body, such as severe burns and occupational poisoning.

The structure selected for the model is $InAs_{0.8}Sb_{0.2}$/InP as suggested by Chichih Liao et. al [7], since InP provide comparatively less lattice mismatch and high thermal conductivity. In our modeling, just like Chichih Liao, we have assumed a thin AlSb/$AlAs_{0.5}Sb_{0.5}$ buffer layers. However we considered that the buffer layer is very thin and will not affect the active region.

2. Modelling of gas detector

In present paper we also used the analytical model characterise the proposed detector as generally used by other researchers [8,9]. In modelling of first part of our analytical modelling, the performance parameters of $InAs_{0.8}Sb_{0.2}$/InP photo detector has been obtained using developed model. Our model includes the lifetime estimation of the carriers in all three major dominant recombination mechanisms, such as AUGER, SRH and Radiative. The detectivity of the photodetector under consideration depends on these dominant mechanisms that control the zero-bias resistance area product of the photodetector (R_0A). Major components of the zero bias resistance area product (R_0A) are diffusion in neutral region, Generation recombination in depletion region and tunnelling component. Two type of tunnelling are possible in narrow band semiconductor photodetectors, BTB (band to band tunnelling) and TAT (Trap assisted tunnelling). Since the trap energy level and its carrier concentration could be intentionally altered by the proper selection of

suitable impurity donor atom and amount of doping, trap assisted tunnelling having main importance in band engineering, so in our model we have focus our main attention on TAT. The model has been applied to estimate different characteristic parameters like detectivity, efficiency etc through R_0A product. In the second task of our modelling, we studied the effect of trap level and N_t-sigma product on characteristic parameters. Emphasis has been given on the investigation of the effect of tunneling via traps and dependence of the resistance-area product of the device on the location of the trap level inside the energy bandgap The importance of this structure lies in the fact that the device based on this structure can be used at room temperature in the range 1.25-1.5 μm i.e. in short-infrared wavelength regions. The detector based on this material has a long wavelength cut-off just above 1.3 μm that makes it suitable for use in optical gas sensors for detection of hydrogen floride HF as NIR spectrum in the region 1.25 to 1.35 micron shows HF and H_2O absorption wavelength [10].

The energy band diagram for the active junction is shown in Fig. 1(b). The top p^+ layer receives the incident light. As said earlier an additional buffer layer is used for lattice matching. The lightly doped n^0 region acts as the active layer. The incident light is absorbed in the neutral regions and depletion region at p^+– n^0 junction. The carriers generated in the neutral p^+ and n^0 regions beyond their respective diffusion lengths would recombine before reaching the junction and fail to contribute to the net photocurrent.

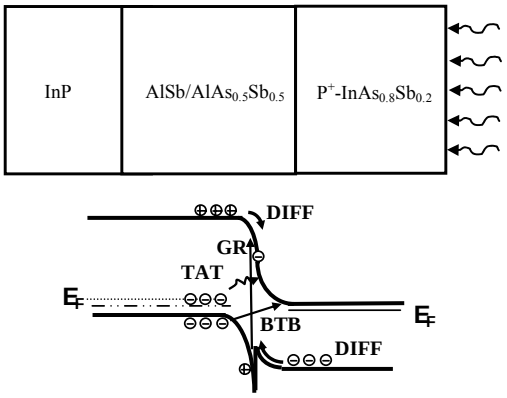

The zero bias resistance area product of the proposed photodetector has been evaluated by considering (i) the diffusion component due to thermally carriers in neutral regions, R_0A_{DIFF}; (ii) Generation-Recombination component of carriers in the depletion region, R_0A_{GR} and (iii) the tunneling component of carriers through the trap level, R_0A_{TUN}. We have not considered BTB component in our modelling. The effective value of the zero-bias resistance area product can be written as

$$R_0A_{NET} = R_0A_{DIFF} + R_0A_{GR} + R_0A_{TUN} \tag{1}$$

2.1. Diffusion component

For the structure under consideration the diffusion current constitutes contributions from both neutral regions, n^0 and p^+. Both minority as well as majority carriers (Hole and electron) constitute the first component of the R_0A Product. The diffusion component of R_0A under the application of a bias voltage, V can be obtained by solving 1-D diffusion equation under appropriate boundary conditions. The diffusion component of R_0A product due to holes and electron respectively can written as [11]

$$(R_0A)_{DIFF_p} = \frac{kTN_D}{q^2 n_{in}^{\ 2}}\frac{\tau_{effp}}{L_p} \frac{\frac{L_pS_p}{D_p}\sinh\left(\frac{d-x_n}{L_p}\right)+\cosh\left(\frac{d-x_n}{L_p}\right)}{\frac{L_pS_p}{D_p}\sinh\left(\frac{d-x_n}{L_p}\right)+\cos\left(\frac{d-x_n}{L_p}\right)}\exp\left[\frac{q(V_{dp}+\Delta E_c)}{kT}\right] \tag{2a}$$

$$(R_0A)_{DIFF_n} = \frac{kTN_A}{q^2 n_{ip}^{\ 2}}\frac{\tau_{effn}}{L_n} \frac{\frac{L_nS_n}{D_n}\sinh\left(\frac{d-x_p}{L_n}\right)+\cosh\left(\frac{d-x_p}{L_n}\right)}{\frac{L_nS_n}{D_n}\cosh\left(\frac{d-x_p}{L_n}\right)+\sinh\left(\frac{d-x_p}{L_n}\right)}\exp\left[\frac{q(V_{dn}+\Delta E_c)}{kT}\right] \tag{2b}$$

In the above equations, N_A and N_D are the acceptor and donor concentrations in p^+ and n^+-regions, respectively, q is the electronic charge, D_p and D_n are the electron and hole diffusion coefficients and L_p and L_n are their respective diffusion lengths, t is the thickness of the InP region and d is the thickness of the n^0-InAsSb active region, x_p and x_n are the width of the depletion regions in p+ and n0 regions respectively. V_{dp} and V_{dn} are the built-in potentials at the P^+–n^0 heterojunction on the n^0 and P^+ side respectively. S_p and S_n are the surface recombination.

2.2 Generation-recombination component

The Generation-Recombination (GR) component of the R_0A product arises not only due to radiative recombination but also due to the indirect or SRH recombination of the thermally generated carriers through the impurity levels arises due to the defects within the depletion region. These intermediate states are referred to as Shockley Read centres or recombination level. The generation-recombination component of current density can be approximated as [11]

$$(R_0A)_{GRn} = \frac{V_{d1}}{2qn_{in}x_n\sigma N_f}\sqrt{\frac{m^*_{en}}{3kT}} \tag{3a}$$

$$(R_0A)_{GRp} = \frac{V_{d2}}{2qn_{ip}x_p\sigma N_f}\sqrt{\frac{m^*_{hp}}{3kT}} \tag{3b}$$

Where, m^*_{en} and m^*_{hp} are the effective mass of electrons and holes in the n^0 and P^+ region respectively, V_{d1} and V_{dp} are barriers due to band bending of n0 region and P^+ region respectively at the P^+–n0 heterointerface, N_f trap density at the P- n^0 heterointerface, n_{ip} is the intrinsic carrier concentration of the P-side and

2.3 Trap-assisted tunneling component

Trap-assisted tunneling occurs when minority carriers tunnel from occupied trap states on the quasi-neutral side to the empty band states on the other side of the junction or though trap sites present in the depletion region of the junction. This mechanism is shown in the energy band diagram of Fig. 1 (b). These trap centres are intermediate energy levels created by the presence of impurities [which may be the intentionally doped] in the material. The trap-assisted tunneling component of current density calculated on the basis of simple one-dimensional model [11] can be written as

$$(R_0 A)_{TUNp} = \frac{K}{qA^*TP_p}\exp\left(q\frac{(v_{d1}+\delta_p)}{kT}\right) \quad (4a)$$

$$(R_0 A)_{TUNn} = \frac{K}{qA^*TP_n}\exp\left(q\frac{(v_{d2}+\delta_n)}{kT}\right) \quad (4b)$$

where A is the effective Richardson constant, P_n and P_p are tunneling factors for of n_0 and P^+-side respectively.

The product of dynamic resistance and area (RA) is given by the reciprocal of the derivative of the current density with respect to voltage.

The net R_0A product for each component is calculated using the following relation

$$\frac{1}{(RA)} = \frac{1}{(RA)_p} + \frac{1}{(RA)_n} \quad (5a)$$

The net or effective value of the resistance area product $(RA)_{NET}$ is given by

$$\frac{1}{(RA)_{NET}} = \frac{1}{(RA)_{DIFF}} + \frac{1}{(RA)_{GR}} + \frac{1}{(RA)_{TAT}} \quad (5b)$$

2.4. Lifetime modelling

In our modelling of we have considered all three dominant recombination processes. These are radiative (which is band-to-band recombination), Auger and Shockley Read–Hall (which are non-radiative) recombination mechanisms. For direct bandgap semiconductors, the lifetime of carriers due to radiative recombination can be obtained by the simple expression

$$\tau_{RAD} = \frac{1}{B_r(n_0 + p_0)} \quad (6)$$

where B_r is the radiative recombination coefficient of the material and n_0 and p_0 are the electron and hole concentrations in the region under thermal equilibrium. On the other hand the non-radiative Auger recombination is quite complex and a non-radiative mechanism. A narrow band semiconductor consisting of a single conduction band and heavy-hole and light-hole valence bands there can be at least ten different types of Auger transitions. Among these transitions, the two most significant transitions that occur at the minimum threshold energy ($E_T = E_g$) are the Auger-1 or CHCC (involving two conduction band electrons and a heavy hole) and Auger-7 or CHLH (involving one conduction band electron and one heavy hole and one light hole). The former is generally dominant in n-type material and the later in p-type material [12]. In the present analysis we have assumed that InAsSb has a band structure similar to that of InSb. For InSb like band structures in which the spin split-off energy approaches the bandgap of the material, another type of Auger transition known as Auger-S or CHSH process also becomes significant. Therefore we have considered the effect Auger-S recombination process for computation of the effective lifetime of the carriers. The net Auger recombination lifetime of the carriers can thus be written as [12]

$$\frac{1}{\tau_{AU}} = \frac{1}{\tau_{A-1}} + \frac{1}{\tau_{A-7}} + \frac{1}{\tau_{A-S}} \quad (7)$$

where τ_{AU} corresponds to the overall value of the mean lifetime of the carriers due to Auger recombination and the other suffixes indicate the components of τ for the corresponding Auger transitions.

The lifetimes for the A-1, A-7, and A-S mechanisms can be written respectively as

$$\tau_{A-1} = \frac{2\tau^i_{A-1}}{1+n_0/p_0} \qquad \tau_{A-7} = \frac{2\tau^i_{A-7}}{1+p_0/n_0}$$

$$\tau_{A-S} = \frac{2\tau^i_{A-S}}{1+p_0/n_0} \quad (8)$$

where p0 and n0 are the majority and minority carrier concentrations at equilibrium state in the active InAsSb region. Here τ^i_{A-1}, τ^i_{A-7}, τ^i_{A-S} indicate the intrinsic recombination times for Auger 1, Auger 7 and Auger S transitions respectively given by [12] as

$$\tau^i_{A-1} = \frac{3.8\times10^{-18}\varepsilon_s^2(1+\mu)^{1/2}(1+2\mu)}{\frac{m^*_e}{m_0}|F_1F_2|^2\left(\frac{kT}{qE_g}\right)^{3/2}}\exp\left[\left(\frac{1+2\mu}{1+\mu}\right)\frac{qE_g}{kT}\right] \quad (9)$$

$$\tau^i_{A-7} = \frac{m^*_e(E_{th})\left(1-\frac{5qE_{th}}{4kT}\right)}{m^*_{e0}\left(1-\frac{3qE_{th}}{2kT}\right)}\tau^i_{A-1} \quad (10)$$

$$\tau^i_{A-S} = \frac{5}{54}\frac{\varepsilon_s^2 m^{*3}_{hh} m^{*3/2}_e kT\Delta^2(E_g+\Delta)}{\pi^4(h/2\pi)^3 q^4 n_i^2 m_s^{5/2}(\Delta-E_g)\exp\left[\frac{q(\Delta-E_g)}{kT}\right]} \quad (11)$$

where q is the electronic charge, μ is the ratio of the conduction band to the heavy-hole valence band effective

mass, εs is the permittivity, F1 and F2 are the overlap integrals of the periodic part of Bloch's functions, me* is the electron effective mass, m0 is the electron rest mass and ni is the intrinsic carrier concentration. Eg and Δ are the energy bandgap and spin-split-off energy of the semiconductor in Joules. Here me* (Eth) represents the electron effective mass corresponding to threshold energy for the Auger 7 transition. For this transition Eth ≈ Eg. For the Auger S transition, mhh* and ms correspond to the heavy hole band effective mass and the spin split-off band effective mass respectively. The lifetime of carriers due to shockley–Read–Hall recombination can be modelled in terms of trap density and capture cross-section as

$$\tau_{SRH} = \frac{1}{\sigma N_f v_{th}} \tag{12}$$

where N_f is the SRH trap density, σ is the capture cross-section and v_{th} is the thermal velocity of the minority carriers in the active region, given by

$$v_{th} = \sqrt{\frac{3kT}{m^*}} \tag{13}$$

m* being the effective mass of the charge carriers.

2.5 Specific detectivity

The most important figure of merit of the MIR photodetector for use in non-telecommunication application is the specific detectivity D*, which depends on the wavelength of incident lightλ, the quantum efficiency η and the zero-bias resistance area product, R_0A. As the dark current of the detector is contributed by three major components e.g., diffusion, generation-recombination and tunneling, the detectivity of the photodetector under consideration should be estimated from the net value of the R_0A product arising out of these mechanisms. The specific detectivity of the photodetector which is a function of the applied voltage can be written as

$$D^* = \frac{q\eta\lambda}{hc}\sqrt{\frac{(RA)_{NET}}{4kT}} \tag{14}$$

where, η is the quantum efficiency, λ is the operating wavelength and $(RA)_{NET}$ is the net or effective value of the zero-bias resistance area product which is a function of the applied voltage.

The quantum efficiency (η) of a p–n junction photodetector has generally three major components. These components arise from the contribution of the three regions e.g., neutral n-region (η_n), neutral p-region (η_p) and the depletion region (η_{dep}) [13] The net quantum efficiency can be obtained by

$$\eta = \eta_n + \eta_p + \eta_{dep} \tag{15}$$

3. Results and iscussion

Numerical computations have been carried out on p^+-$InAs_{0.8}Sb_{02}/n^0$-InP photodetector at room temperature (300K). The light has been assumed to be incident from the top p+-$InAs_{0.8}Sb_{0.2}$ side. The incident photons with energy higher than the band gap of $InAs_{0.8}Sb_{0.2}$ are absorbed in both p+ and n0 regions. Various other parameters used in the theoretical computations are taken from references [14], [15] and are listed in Table 1.

The different components of the dark current and the R_0A products have been calculated using the theoretical model discussed above.

Table 1. Parameter values used in the computation.

Parameter	values
N_D	10^{22} m^{-3}
N_f	10^{20} m^{-3}
t	3 μm
d	1 μm
ε_r ($InAs_{1-x}Sb_x$)	(15.15+1.65x)
m_n^* ($InAs_{1-x}Sb_x$)	0.023-0.039x+0.03x^2 m_0
m_p^* ($InAs_{1-x}Sb_x$)	0.41+0.02x m_0
χ_{InAsSb}	4.9-0.31x eV
Δ ($InAs_{1-x}Sb_x$)	0.39+0.42x
D_n($InAs_{1-x}Sb_x$)	10^{-1} m^2/s
D_p($InAs_{1-x}Sb_x$)	10^{-3} m^2/s

In present work the dependence of the RA product as well as the major parameters of the gas detectors such as Detectivity and quantum efficiency on the applied voltage and trap densities has been estimated quantitatively. The Fig. 2 shows the variation of the Net Dark current along with its component due to major three recombination mechanism (diffusion, generation-recombination and tunnelling) with the applied bias voltage. This plot is obtained for the trap level E_t = 1.33 eV. Plot shows that the generation recombination (GR) component is the dominant component of the net dark current. Whereas diffusion components of current having negligible contributions on net current.

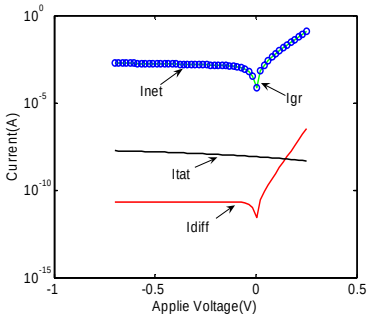

Fig. 2. Variation of the net Dark current along with its component with the applied bias voltage.

The net current and its component having dip at zero bias and increased in forward bias due to biasing. In Fig. 3, the variation of R_0A_{net} and its component for the same E_t = 1.33eV, is shown with applied voltage. As obvious, the R_0A_{net} value depends on the GR component except at large reverse bias where it is slightly affected by TAT component. Actual nature of the I-V characteristic of the detector is largely dependent on the processing history of the device. In devices fabricated with a large number of traps, the reverse saturation current does not remain constant and independent of reverse voltage as suggested by Chakrabarti et.al [6]. This nature is attributed to trap-assisted tunneling that occurs via the defects in the device. The contribution of the trap-assisted tunneling component however, depends on the number of trap centres as well as the location of the trap level inside the forbidden energy gap. (it is illustrate in Fig. 4, in which the variation of the Zero-bias area product(R_0A) with applied voltage is plotted for the four different value of Nt (1×10^{18}, 1×10^{20} ,1×10^{22}, and 1×10^{24}). This plot shows that the generation recombination (GR) component and TAT component is dominant net R_0Acomponent but diffusion components of zero-bias area product having negligible contributions with net area product. Trap energy level E_t measured in electron volts and indicates positions of the trap levels measured from the valence band-edge within the forbidden energy bandgap. However when the trap density decreases from 10^{24} m^{-3} to 10^{18} m^{-3} the dependence of R_0A product will start governing by the TAT component. This decreases the overall value of the net resistance area product and in turn detectivity.

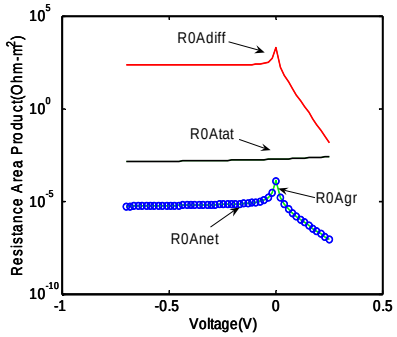

Fig. 3. Variation of the Zero Bias Resistance area Product along with its component with applied bias voltage.

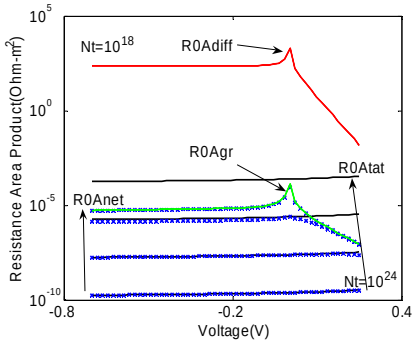

Fig. 4. Variation of the net R_0A with applied voltage for different value of Nt.

In diffusion component is not affected by the trap density since it is mainly due to the carriers coming at the depletion edge from the neutral region.

In Fig. 5, the variation of the Zero-bias area product(R_0A) with applied voltage is plotted for the four different value of N_f * sigma product (0.01, 0.1 , 1 and 10) are shown. We found that the net zero bias resistance area product is very sensitive to N_f * sigma product indicated as P in the figure. As we increase P value by either increasing N_f (Trap carrier density) or by increasing sigma (Capture cross section area) the value of net resistance area P Product (R_0A_{net}) increases more than 10^3 times. Since R_0A directly proportional to detectivity directly it also decreases. So by monitoring and selecting Nf * sigma product properly one can modify the detectivity of the detector.

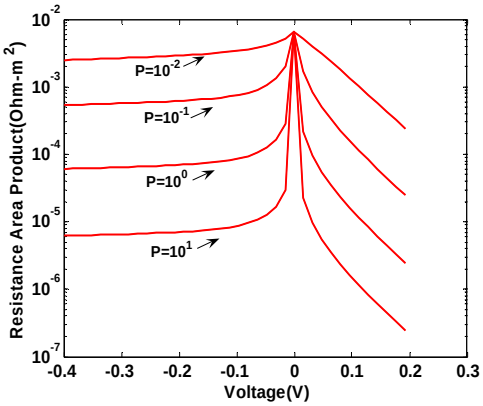

Fig. 5. Variation of the net R_0A with applied voltage different value of P.

Fig. 6 shows the efficiency of the detector with respect to operating wavelength. Here efficiency having its maximum value 1.55 at wavelength 1.35 µm and decreases sharply on the both side. So the device operates well between the wavelength ranges 1.25 to 1.50 µm. Here we found that for the high effective concentration of trap carrier N_f the Net R_0A peak and its position is shifted towards positive applied voltage thus the device will perform well for low reverse voltage operation. Also as the N_f value effect the Net R_0A peak it will in turn affect detectivity of the photodetector as the square root of R_0A is directly related with Detectivity. At low donor concentration responsivity remains constant but for large doping $<10^{24}$ m^{-3} responsivity start decreasing with donor concentration and affect the detectivity of the gas detector. The plot in Fig. 7, the variation of the detectivity of the gas detector with operating wavelength for different value of doping material of energy E_t (E_t=1.8 , E_t=2.4 and E_t=3.0) is shown. Figure shows that the large detectivity 2.0×10^6 $mHz^{1/2}/W$ is observe at wavelength 1.37 µm. Detectivity sharply decreases towards both sides. The value of the trap level affects the detectivity of the detector. With low E_t value detectivity plot becomes slightly sharper. Therefore with proper choice of trap level we can slightly tune the

detectivity of the gas detector for the characteristic wavelength of the target gas.

In a last plot in Fig. 8, the variation of the detectivity of the gas detector with operating wavelength for four different value of N_t-sigma product (1×10^{-2}, 1×10^{-1}, 1×10^{-0}, and $1\times10^{1)}$ is shown. Figure shows that the large detectivity 2.0×10^6 $mHz^{1/2}/W$ is observe at wavelength 1.37 µm. Detectivity sharply decreases towards both sides. The value of N_t-sigma product affects the detectivity of the detector.

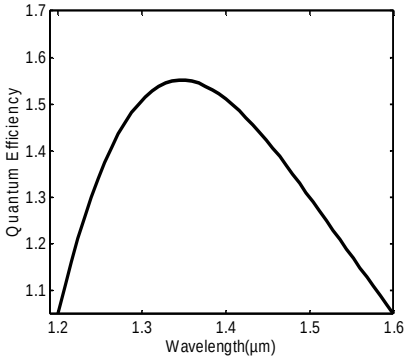

Fig. 6. Efficiency of the detector with respect to operating wavelength.

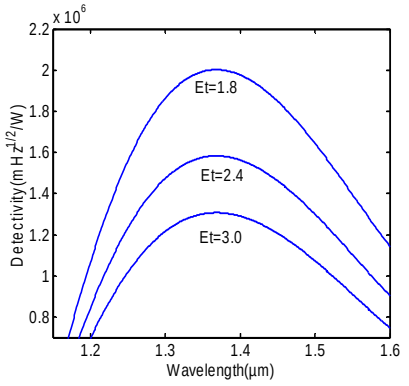

Fig. 7. Variation of the detectivity with operating wavelength at different e_t.

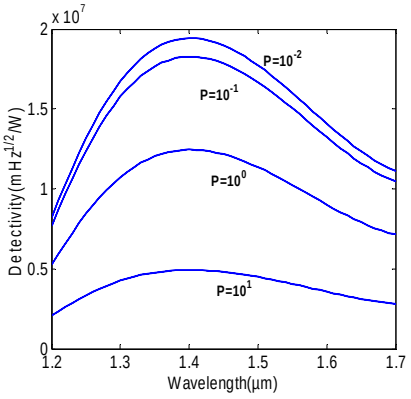

Fig. 8. Variation of the detectivity with operating wavelength for different value of P.

4. Conclusion

In this paper a generic model of a mid-infrared gas detector based on InP (100) semiconductor has been resented. The model has been applied to characterise theoretically an InP/$InAs_{0.2}Sb_{0.8}$ P^+–n^0 gas detector. The study reveals that the basic as well as end parameters of the detector is largely affected by the trap levels, which may be intentionally incorporated in the detector using suitable doping material (of energy E_t) at the time of fabrication. Results obtained on the basis of the model clearly indicate that the device parameter and the performance of the detector can be optimising by tap level. A very high detectivity slightly above than $D= 2.0 \times 10^6$ is $mHz^{1/2}/W$ obtained at the wavelength 1.35 µm on the basis of the model. Design engineers can use the model presented here as a tool for detecting the presence of trap centre in the processed device. The model can also be used for optimization detector for a particular gas, which in turn reduces the number of experimental trials required for the development of improved photodetectors with sharp detection peak.

References

[1] W. W. Anderson, Infrared Phys., **20**, 363 (1980).
[2] A. Rogalski, K. Adamiec, J. Rutkowski, SPIE Press, Bellingham, USA (2000).
[3] H. H. Gao, A. Krier, V. V. Sherstnev, Applied Phys. Lett., **77,** 872 (2000).
[4] M. Mello, B. Poti1, A. Risi, A. Passaseo De, M. Lomascolo, M. De Vittorio, J. Opt. A: Pure Appl. Opt., **8**, S545 (2006).
[5] M. A. Afrailov, Infrared Physics & Technology, **53**, 29 (2010).
[6] P. Chakrabarti, P. K. Saxena, R. K. Lal, International J. Infrared and Millimeter waves, **27**, 1119 (2006).
[7] Chichih Liao, Bing-Ruey Wu, K. C. Hsieh, K. Y. Cheng, J. Vac. Sci. Technol. B, No. 3, 26 (2008).
[8] H. Shao, W. Li, A. Torfi, D. Moscicka, W. I. Wang, IEEE Photonics Technology Letters, **18**, 16 (2006).
[9] A. D. D. Dwivedi, A. Mittal, A. Agrawal, P. Chakrabarti, Infrared Physics and Technology, **53**, 236 (2010).
[10] K. L. McNesby, R. Reed Skaggs, A. W. Miziolek, M. Clay, S. H. Hoke, C. S. Miser, Applied Physics B: Lasers and Optics, **67**(4), 443 (1998).
[11] R. K. Lal, M. Jain, S. Gupta, P. Chakrabarti, IEE Proceedings Optoelectronics, **150**, 527 (2003).
[12] V. Gopal, S. K. Singh, R. M. Mehra, Infrared Physics and Technology, **43**, 317 (2002).
[13] R. K. Lal, M. Jain, S. Gupta, P. Chakrabarti, Infrared Physics and Technology, **44**, 125 (2003).
[14] M. Levinshtein, S. Rumyantsev, M. Shur, (Eds.): 1 and 2, World Scientific, London (1999).
[15] A. Rakovska, V. Berger, X. Marcadet, B. Vinter, K. Bouzehouane, D. Kaplan, Semiconductor Science and Technology, **15**, 34 (2000).

*Corresponding author: rklal@bitmesrs.ac.in